Synthesis of Heavy Elements in a Helium Star of 32 $M_\odot$ inside a Jet of Supernova Explosion

Masaomi ONO[1], Masa-aki HASHIMOTO[1], Yukihiro KIKUCHI[1], Shin-ichiro FUJIMOTO[2] and Kenzo ARAI[3]

[1]*Department of Physics, Kyushu University, Fukuoka 812-8581*
[2]*Kumamoto National College of Technology, Kumamoto 861-1102*
[3]*Department of Physics, Kumamoto University, Kumamoto 860-8555*

(Received September 30, 2010)

We investigate synthesis of heavy elements in a helium star of 32 $M_\odot$. Numerical calculations of nucleosynthesis have been performed during the stage of hydrostatic stellar evolution. A collapsar model is adopted whose jets are driven by magneto-hydrodynamical effects of differentially rotating core. Nucleosynthesis inside the jets is followed along the trajectories of tracer particles. Both results of hydrostatic and explosive nucleosyntheses are combined to be the yields after supernoca explosion. Comparing with the solar system abundances, we find appreciable overproduction for nuclei of the mass number $60 < A < 200$.

§1. Introduction

The origin of most elements heavier than carbon in the universe has been attributed to the supernova explosions. Unfortunately, the mechanism of the supernova explosion is not clear, because multi-dimensional hydrodynamics coupled to neutrino transport cannot be solved numerically without some approximations. Massive stars larger than 8 $M_\odot$ evolve to form the Fe-core composed of iron-group nuclei. The Fe-core grows and eventually begins to collapse, which will lead to supernova explosion. On the other hand, it has been suggested[1)] that a star of more massive than 25 $M_\odot$ may collapse to a black hole (BH). A collapsar model[2)] was presented as one of the mechanism to produce a relativistic jet of γ-ray bursts, where an accretion disk around the BH may be crucial to induce jets.[3)]

Magnetohydrodynamic (MHD) simulations have been performed in the context of a collapsar model and clarify the formation of a jet due to the pressure of the collimated magnetic field that is twisted by the strong differential rotation.[4)] Furthermore, nucleosynthesis has been calculated for the jets that run through the Fe-core.[5)] However, since the calculations have been done for the newly synthesized materials inside the jets, it is not enough for precise comparison with the solar system abundances. Therefore, we have performed detailed calculations of nucleosynthesis during the hydrostatic evolution of a 32 $M_\odot$ helium star with a relatively large network which includes 464 nuclei.[6)]

In the present paper, we investigate detailed nucleosynthesis during the jet explosion of the 32 $M_\odot$ helium star that corresponds to 70 $M_\odot$ in the main sequence stage. We use the results of the MHD simulation of a collapsar with initial distributions of angular velocity and magnetic field implemented. Heavy-element synthesis is calculated using a specific collapsar model that has exploded as jets. Both results of hydrostatic and explosive nucleosynthesis are combined to be "exact" yields after supernova explosion.

§2. MHD model

We adopt the MHD model R51 which has been constructed in previous studies.[6] For completeness, we summarize briefly the numerical method, input physics and the initial model.

2.1. *Numerical method and input physics*

The MHD equations that simulate jet formation and ejection are as follows:

$$\frac{D\rho}{Dt} + \rho\nabla \cdot \boldsymbol{v} = 0, \tag{2.1}$$

$$\rho\frac{D\boldsymbol{v}}{Dt} = -\nabla P - \rho\nabla\Big(\Phi - \frac{GM_{\rm BH}}{r - r_g}\Big) + \frac{1}{4\pi}(\nabla \times \boldsymbol{B}) \times \boldsymbol{B}, \tag{2.2}$$

$$\rho\frac{D}{Dt}\Big(\frac{e}{\rho}\Big) = -P\nabla \cdot \boldsymbol{v} - \varepsilon_\nu, \tag{2.3}$$

$$\frac{\partial \boldsymbol{B}}{\partial t} = \nabla \times (\boldsymbol{v} \times \boldsymbol{B}), \tag{2.4}$$

$$\nabla^2\Phi = 4\pi G\rho, \tag{2.5}$$

where ρ is the mass density, $\boldsymbol{v}$ the fluid velocity, P the pressure but for the magnetic pressure, Φ the self gravitational potential, G the gravitational constant, $M_{\rm BH}$ the BH mass, $r_g = 2GM_{\rm BH}/c^2$ the Schwarzschild radius, $\boldsymbol{B}$ the magnetic field, e the internal energy density, ε_ν the neutrino energy loss rate and D/Dt the Lagrange derivative.

Spherical coordinates (r, θ, ϕ) are adopted under the assumption of the symmetries about the rotational axis and with respect to the equatorial plane. The polar angle is set to be $0 < \theta < \pi/2$ and the radius covers the region from the absorption boundary $r_{\rm in}$ to 3×10^4 km. BH is replaced with a point source at the center and its mass is taken as the mass inside the radius $r_{\rm in}$ = 50 km (extended to 100 km at the late stage of the simulation). Therefore, all the matter accreted through the boundary is added to the point source. Let the time step of the calculation be Δt, the growth in the mass of the point source is

$$\Delta M = \Delta t\, 4\pi r_{\rm in}^2 \int_0^{\pi/2} \rho v_r \sin\theta d\theta, \tag{2.6}$$

where v_r and ρ are the radial infall velocity and density, respectively, at the boundary.

We use a non-relativistic MHD code of ZEUS-2D[7] to simulate the explosion due to magnetic field coupled with differential rotation. The gravitational collapse is followed, using a realistic equation of state (EOS).[8] For a low density region of ρ $< 10^5$ g cm^{-3}, we take another EOS connected smoothly at the density boundary, which consists of the non-relativistic ions, partially degenerate relativistic electrons and radiation.[9]

As for the neutrino loss rate for $\rho \leq 10^{12}$ g cm^{-3}, we consider three processes:

$$p + e^- \longrightarrow n + \nu_e \; ; \quad n + e^+ \longrightarrow \bar{\nu}_e + p,$$

$$e^+ + e^- \longrightarrow \nu_i + \bar{\nu}_i,$$

$$n + n \longrightarrow n + n + \nu_i + \bar{\nu}_i,$$

with $i = e$, μ, τ. These are electron-positron pair capture on nuclei (URCA process), electron-positron pair annihilation and nucleon-nucleon bremsstrahlung.[10]

If density becomes high for neutrinos to be opaque, we use the two-stream approximation[11] that includes the effects of neutrino trapping.

2.2. *Initial conditions*

Using the physical quantities of the density, temperature, and electron mole number given in the presupernova model of a 32 $M_\odot$ helium core,[12] we have constructed precollapse models whose initial quantities of the pressure, internal energy density and entropy have been implemented in ZEUS-2D. Since these precollapse models are in spherical symmetry, we specify the initial configurations of both angular velocity and magnetic field. The initial angular velocity is written as:[13]

$$\Omega = \Omega_0 \frac{r_0^2}{r^2 + r_0^2}, \tag{2.7}$$

where $\Omega_0 = 5$ s^{-1} and $r_0 = 1500$ km.

The initial toroidal magnetic field is given by

$$B_\phi = B_0 \frac{r_0^2}{r^2 + r_0^2}, \tag{2.8}$$

where $B_0 = 5.7 \times 10^{12}$ G. We also set uniform poloidal magnetic field initially in the direction of the rotational axis, $B_Z = 5 \times 10^{11}$ G.

2.3. *Ejection of matters due to jets*

The final time of R51 is $t_f = 1.504$ s and the central black hole grows to $M_{\rm BH}=$ 1.9 $M_\odot$. Ejection of mass and energy due to the jet is limited to the range $0 < \theta \leq \pi/6$ at a large distance, where the ejection rates decrease more than an order of magnitude for $\theta > \pi/6$. The ejection rates of mass and energy at distance r_i are

$$\dot{M}_{\rm ej} = 4\pi r_i^2 \int_0^{\pi/6} \rho v_{\rm jet} \sin\theta \, d\theta, \tag{2.9}$$

$$\dot{E}_{\rm ej} = 4\pi r_i^2 \int_0^{\pi/6} \left(\frac{1}{2}\rho v^2 + \frac{1}{8\pi} B^2 + e \right) v_{\rm jet} \sin\theta \, d\theta, \tag{2.10}$$

where r_i ($i = 1 - 20$) is selected between 1×10^8 and 2.8×10^9 cm. The ejection velocity $v_{\rm jet}$ is chosen as

$$v_{\text{jet}} = \begin{cases} v_r & (v_r > 0.01\,c) \\ 0 & (v_r < 0.01\,c), \end{cases} \tag{2.11}$$

where the lower limit is taken to be $0.01c$, since matters with lower velocities cannot exceed the corresponding escape velocity, which is around 10^9 cm s^{-1} for a core of about $1\,M_\odot$. The mass $M_{\rm ej}$ and the energy $E_{\rm ej}$ of the jet amount to $0.124\ M_\odot$ and 3.02×10^{51} erg, respectively. The average rates of mass and energy ejection, (2.9) and (2.10), are $4.77\times10^{-2}\ M_\odot\ s^{-1}$ and 2.17×10^{50} erg s^{-1}, respectively.

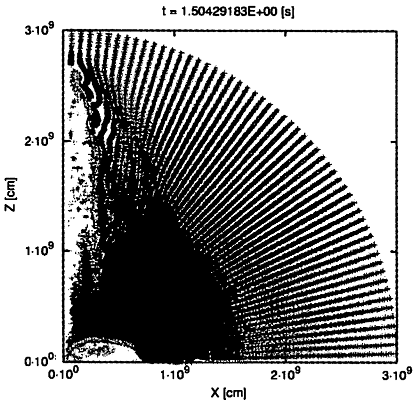

Fig. 1. Distribution of the tracer particles on the xz-plane at the end of the simulation, t_f = 1.504 s.

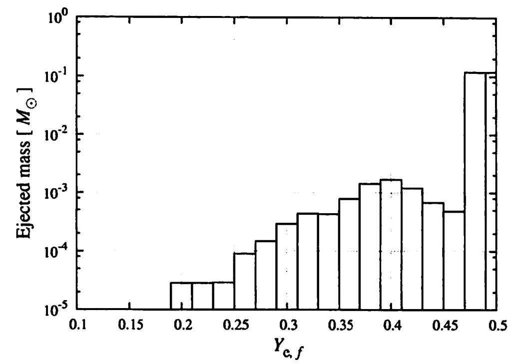

Fig. 2. Distribution of the ejected mass against the electron fraction $Y_{{\rm e},f}$ for ejected tracer particles.

2.4. *Nucleosynthesis inside the MHD jet*

In calculating nucleosynthesis inside the MHD jet, two thousand tracer particles are distributed over the region between 10^2 and 3×10^4 km from the center which covers out of the deep Fe-core to the inner oxygen-rich layer. The Lagrange evolution of density and temperature of each tracer particle can be obtained from the method in Ref. 5), of which we can calculate nucleosynthesis and follow the change in composition. Figure 1 shows the distribution of the tracer particles at the end of the simulation. Particles that appear deep inside the original Fe-core ($\rho \geq 10^{10}$ g cm^{-3}) suffer from electron captures. Therefore, we calculate the change in the electron fraction $Y_{\rm e}$ of the ejected tracer particles due to the weak interactions of $e^\pm$ captures and $\beta^\pm$ decays until the last stage of the nuclear statistical equilibrium (NSE) before the calculation. The change in $Y_{\rm e}$ is given by[14)]

$$\frac{dY_{\rm e}}{dt} = \sum_i (\lambda_+ - \lambda_-) y_i, \tag{2.12}$$

where λ_+ contains the β^- and positron capture rates and λ_- is the β^+ and electron capture rates. Figure 2 shows the distribution of the ejected mass in $M_\odot$ aginst the electron fraction $Y_{{\rm e},f}$ of ejected particles at the end of NSE.

Table I. Nuclide contained in the two networks of ETFSI and FRDM.

Nuclide	ETFSI A	FRDM A	Nuclide	ETFSI A	FRDM A
H	1 – 3	1 – 3	Sb	102 – 161	119 – 162
He	3 – 6	3 – 6	Te	104 – 164	120 – 164
Li	6 – 8	6 – 8	I	110 – 165	123 – 171
Be	7 – 12	7 – 12	Xe	112 – 168	124 – 180
B	8 – 14	8 – 14	Cs	114 – 181	129 – 181
C	9 – 18	11 – 18	Ba	117 – 182	130 – 182
N	11 – 21	12 – 21	La	120 – 183	135 – 183
O	13 – 22	14 – 22	Ce	126 – 184	136 – 184
F	14 – 26	17 – 26	Pr	127 – 185	141 – 185
Ne	15 – 34	17 – 30	Nd	132 – 186	142 – 186
Na	17 – 37	20 – 34	Pm	133 – 187	143 – 187
Mg	19 – 38	20 – 36	Sm	136 – 188	144 – 188
Al	21 – 41	22 – 41	Eu	137 – 193	151 – 189
Si	22 – 46	24 – 44	Gd	149 – 196	152 – 190
P	23 – 49	27 – 45	Tb	143 – 197	155 – 198
S	24 – 50	28 – 48	Dy	146 – 202	156 – 212
Cl	26 – 51	31 – 51	Ho	149 – 203	161 – 215
Ar	27 – 54	32 – 56	Er	151 – 208	162 – 216
K	30 – 57	35 – 55	Tm	152 – 215	167 – 221
Ca	32 – 60	36 – 62	Yb	154 – 218	168 – 222
Sc	34 – 67	39 – 67	Lu	156 – 225	173 – 224
Ti	36 – 72	40 – 70	Hf	158 – 228	174 – 226
V	38 – 76	43 – 73	Ta	164 – 229	179 – 235
Cr	40 – 78	44 – 74	W	166 – 232	180 – 236
Mn	42 – 81	46 – 77	Re	168 – 235	183 – 239
Fe	43 – 84	47 – 78	Os	170 – 236	184 – 240
Co	45 – 85	50 – 81	Ir	172 – 239	189 – 241
Ni	47 – 86	51 – 82	Pt	174 – 243	190 – 242
Cu	49 – 89	56 – 91	Au	178 – 247	195 – 247
Zn	52 – 92	57 – 94	Hg	180 – 251	196 – 258
Ga	54 – 97	60 – 95	Tl	186 – 255	203 – 263
Ge	56 – 100	61 – 102	Pb	190 – 259	204 – 264
As	58 – 101	64 – 103	Bi	192 – 263	209 – 265
Se	60 – 104	65 – 106	Po	210 – 267	210 – 266
Br	62 – 117	68 – 117	At	211 – 269	211 – 269
Kr	64 – 118	69 – 118	Rn	215 – 270	215 – 270
Rb	68 – 119	74 – 119	Fr	218 – 271	218 – 271
Sr	70 – 120	77 – 120	Ra	221 – 272	221 – 272
Y	72 – 121	79 – 121	Ac	224 – 273	224 – 273
Zr	74 – 124	81 – 122	Th	227 – 274	227 – 274
Nb	78 – 129	83 – 125	Pa	230 – 277	230 – 278
Mo	80 – 132	86 – 126	U	232 – 280	232 – 280
Tc	82 – 133	90 – 129	Np	235 – 284	235 – 284
Ru	84 – 136	96 – 130	Pu	238 – 288	238 – 287
Rh	87 – 137	101 – 141	Am	241 – 292	241 – 290
Pd	90 – 138	102 – 142	Cm	–	244 – 294
Ag	92 – 147	105 – 149	Bk	–	247 – 298
Cd	94 – 148	106 – 150	Cf	–	250 – 302
In	96 – 149	111 – 155	Es	–	253 – 306
Sn	100 – 154	112 – 156	Fm	–	256 – 310

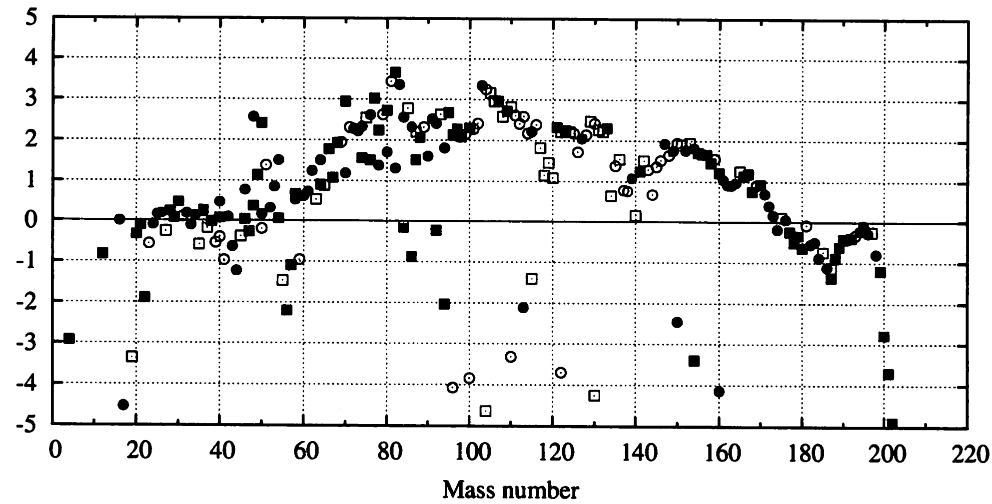

Fig. 3. Normalized overproduction factors of nuclei produced by the jet explosion with use of the mass formula ETFSI. The filled and open squares indicate the isotopes with even and odd atomic numbers, respectively.

To investigate the heavy-element synthesis, we calculate nucleosynthesis with respect to the ejected particles using a large nuclear reaction network, where the reaction rates are based on the mass formula of the extended Thomas-Fermi plus Strutinsky integral (ETFSI)[15] which includes 4463 nuclei up to ^{292}Am. We also calculate nucleosynthesis with a network based on the mass formula of the finite-range droplet model (FRDM)[16] which includes 4071 nuclei up to ^{310}Fm. The two networks are shown in Table I. Finally, to compare with solar abundances, both results of hydrostatic and explosive nucleosynthesis are combined to be the yields after supernoca explosion.

§3. Results and discussion

We compare the produced elements calculated from two networks with the solar system abundances. The normalized overproduction factor relative to ^{16}O is defined as $[X_i/^{16}\mathrm{O}] = \log[\,(X(i)/X(^{16}\mathrm{O}))\,] - \log[\,(X(i)/X(^{16}\mathrm{O}))_\odot]$, where $X(i)$ denotes the mass fraction of i-th nuclei. Figure 3 shows the overproduction factors against mass number with use of the mass formula ETFSI. The filled and open squares indicate the isotopes with even and odd atomic numbers, respectively. Note that neutron-rich elements of $45 < A < 55$ and $60 < A < 140$ are highly overproduced. The overproduced elements of $140 < A < 200$ are due to the ejected matter which have low $Y_{\mathrm{e},f}$ around 0.2 as shown in Fig. 2, from which ejected materials undergo the r-process nucleosynthesis. The overproduced elements of $A > 90$ are primaly synthesized in the jet. The overproduction factor has a peak at $A = 195$, of which the mass number correspond to the neutron magic number of 126. The stable elements of $60 < A < 90$ are overproduced significantly, which is due to the weak s-process in the hydrostatic evolution. In contrast, the stable nuclei of $A > 90$ are underproduced and they could be compensated by the products of the s-process in the relatively low mass AGB stars.

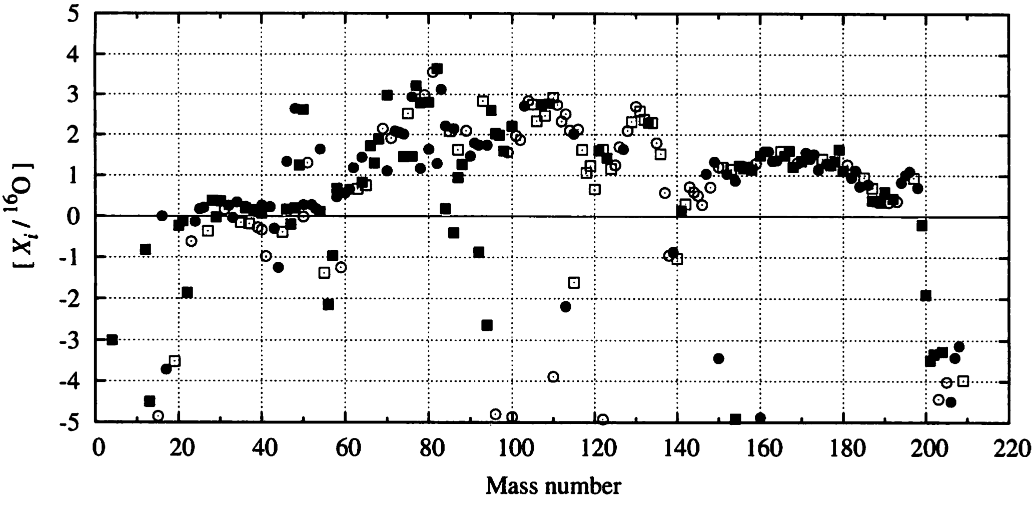

Fig. 4. Same as Fig. 3 but for the mass formula FRDM.

In Fig. 4, we show the overproduction factors calculated with the network of the mass formula FRDM. Neutron rich elements of $60 < A < 140$ are overproduced as in the case of ETFSI, but the elements of $140 < A < 200$ are more abundant than that of ETFSI. The overabundances are more outstanding at $A = 130$ than that of ETFSI, which corresponds to the nutron magic number of 82. These differences are mainly due to the difference in the neutron drip line.

Overall, our supernova explosion model produces the neutron-rich elements of $70 < A < 140$ and weak s-elements of $70 < A < 90$. The overproduction level is within the 2 – 3 orders of magnitude and the total ejected mass of this jet-like explosion model could be around 1 $M_\odot$, which is one order of magnitude less than that of spherical explosion models. Therefore, our model could correspond to rare case and the event rate could be 1 – 2 orders of magnitude less than that of usual supernova explosion models. Other underproduced elements would be ascribed to different types of supernovae.

In the present paper, we have considered the elements of $A < 90$ in the hydrostatic nucleosynthesis. Therefore, we may underestimate the stable nuclei of $A > 90$. We should investigate the full s-process in the hydrostatic evolution stage, where the following input physics on nuclear processes is important: exprimental nuclear reaction rates of neutron capture processes around stabe nuclei, beta decay rates from thermally excited states, separate treatment of long-lived isomeric states. Convection in hydrostatic stellar evolution should be impotant ingredients for the s-process. Related to the s-process, we will study the p-process in the explosive nucleosynthesis in future, where the seeds of s-elements directly affect the yeilds of p-elements.

Acknowledgments

This work has been supported in part by a Grant-in-Aid for Scientific Research (19104006, 21540272) of the Ministry of Education, Culture, Sports, Science and Tecnology of Japan.

References

1) A. Heger et al. Astrophys. J. **591** (2003), 288.
2) S. E. Woosley, Astrophys. J. **405** (1993), 273.
3) A. I. MacFadyen and S. E. Woosley, Astrophys. J. **524** (1999), 262.
4) S. Koide, K. Shibata, T. Kudoh and D. L. Meier, Science **295** (2002), 1688.
D. Proga, A. I. MacFadyen, P. J. Armitage and M. C. Begelman, Astrophys. J. **599** (2003), L5.
Y. Mizuno, S. Yamada, S. Koide, and K. Shibata, Astrophys. J. **615** (2004), 389.
S. Fujimoto, K. Kotake, S. Yamada, M. Hashimoto and K. Sato, Astrophys. J. **644** (2006), 1040.
S. Nagataki, R. Takahashi, A. Mizuta and T. Takiwaki, Astrophys. J. **659** (2007), 512.
5) S. Fujimoto, M. Hashimoto, K. Kotake and S. Yamada, Astrophys. J. **656** (2007), 382.
S. Fujimoto, N. Nishimura and M. Hashimoto, Astrophys. J. **680** (2008), 1350.
6) M. Ono, M. Hashimoto, S. Fujimoto and K. Arai, Phys, Rep. Kumamoto Univ. **13** (2008), 33.
M. Ono, M. Hashimoto, S. Fujimoto, K. Kotake and S. Yamada, Prog. Theor. Phys. **122** (2009), 755.
7) J. M. Stone and M. L. Norman, Astrophys. J. Suppl. **80** (1992), 753; *ibid.* 791.
8) H. Shen, H. Toki, K. Oyamatsu and K. Sumiyoshi, Nucl. Phys. **A637** (1998), 435.
K. Kotake, H. Sawai, S. Yamada and K. Sato, Astrophys. J. **608** (2004), 391.
9) N. Yasutake, K. Kotake, M. Hashimoto and S. Yamada, Phys. Rev. **D75** (2007), 084012.
10) T. Di Matteo, R. Perna and R. Narayan, Astrophys. J. **579** (2002), 706.
11) R. Popham and R. Narayan, Astrophys. J. **442** (1995), 337.
12) M. Hashimoto, Prog. Theor. Phys. **94** (1995), 663.
13) A. Heger, S. E. Woosley, N. Langer and H. C. Spruit, Proceedings of IAU Symp. **215** (2004), 591.
14) S. Nishimura, K. Kotake, M. Hashimoto, S. Yamada, N. Nishimura, S. Fujimoto and K. Sato, Astrophys. J. **642** (2006), 410.
15) S. Goriely, F. Tondeur and J. M. Pearson, Atomic Data and Nuclear Data Tables, **77** (2001), 311.
16) P. Möller, J. R. Nix, W. D. Myers and W. J. Swiatecki, Atomic Data and Nuclear Data Tables, **59** (1995), 185.